

Effect of the growth rate on the morphology and structural properties of hut-shaped Ge islands in Si(001)

A I Yakimov¹, A I Nikiforov¹, A V Dvurechenskii¹, V V Ulyanov¹,
V A Volodin¹ and R Groetzschel²

¹ Institute of Semiconductor Physics, Siberian Branch of the Russian Academy of Sciences,
630090 Novosibirsk, Russia

² Research Center Rossendorf, Institute for Ion Beam Physics and Material Research, Dresden,
D-01314, Germany

E-mail: yakimov@isp.nsc.ru

Received 15 June 2006, in final form 13 August 2006

Published 1 September 2006

Online at stacks.iop.org/Nano/17/4743

Abstract

The effect of Ge deposition rate on the morphology and structural properties of self-assembled Ge/Si(001) islands was studied. Ge/Si(001) layers were grown by solid-source molecular-beam epitaxy at 500 °C. We adjusted the Ge coverage, 6 monolayers (ML), and varied the Ge growth rate by a factor of 100, $R = 0.02$ – 2 ML s^{-1} , to produce films consisting of hut-shaped Ge islands. The samples were characterized by scanning tunnelling microscopy, Raman spectroscopy, and Rutherford backscattering measurements. The mean lateral size of Ge nanoclusters decreases from 14.1 nm at $R = 0.02 \text{ ML s}^{-1}$ to 9.8 nm at $R = 2 \text{ ML s}^{-1}$. The normalized width of the size distribution shows non-monotonic behaviour as a function of R and has a minimum value of 19% at $R = 2 \text{ ML s}^{-1}$. Ge nanoclusters fabricated at the highest deposition rate demonstrate the best structural quality and the highest Ge content (~ 0.9).

1. Introduction

Ge on Si(001) (4.2% lattice mismatch) is one of the intensively studied systems exhibiting a self-organization of nanostructures in semiconductor heteroepitaxy. Electronic and opto-electronic nanodevices implemented on Ge self-assembled quantum dots (QDs) in a Si matrix have attracted much attention due to their compatibility with modern Si-based complementary metal-oxide–semiconductor circuitry. This would offer a substantial reduction in complexity and cost of future high performance electronics. In many applications, the control of the size, density and composition of Ge islands on the stage of growth is essential. Several approaches have been exploited to tune the morphology and structural properties of Ge QDs, such as manipulating the Ge growth [1] and overgrowth [2] temperatures, the Ge coverage [3], vertical ordering in QD multilayers [4–6], surfactant-mediated growth [7, 8], deposition on vicinal [9] and oxidized [10] surfaces, and ion-beam stimulated growth [11].

Another parameter which can control the formation of QDs through the kinetic factors is the dot deposition rate R . Little work has been done on the influence of grown rate on the formation of Ge/Si(001) nanoclusters. Recently, Cho *et al* [12] demonstrated the effect of the deposition rate on the spatial distribution of dome-shaped Ge islands fabricated at high (600 °C) temperature. McDaniel *et al* [13] reported on the increase in Ge composition as the deposition rate increases also for dome clusters grown at 650 °C. The situation in all cases was complicated by shape transitions between pyramids and domes. In this paper we focus our study on small (<15 nm) Ge nanoislands which were grown at lower temperature (500 °C) and have the form of well-defined hut clusters.

2. Sample preparation

Samples were grown by solid-source molecular-beam epitaxy on a p-Si(001) substrate. We varied the Ge deposition rate from $R = 0.02$ to 2 ML s^{-1} while maintaining the substrate

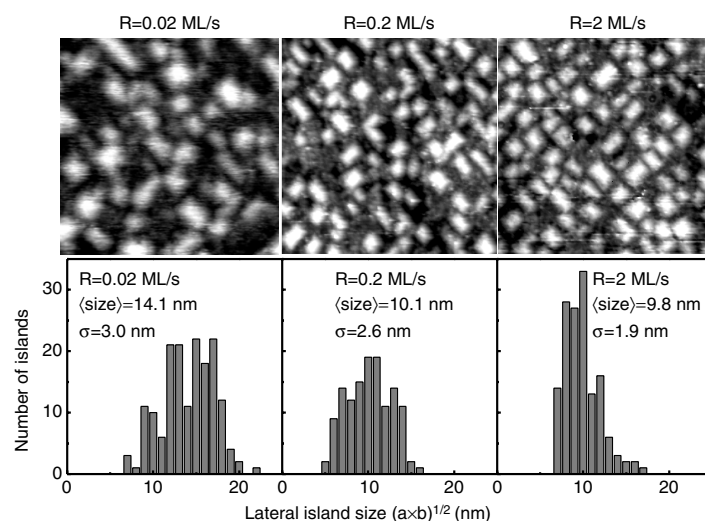


Figure 1. A series of $150 \times 150 \text{ nm}^2$ STM images and size distribution histograms of Ge islands deposited at a substrate temperature of 500°C with varying Ge deposition rates. The amount of Ge deposited is 6 ML.

temperature, $T_s = 500^\circ\text{C}$, and the Ge coverage, 6 monolayers (ML, $1 \text{ ML} = 6.27 \times 10^{14} \text{ Ge atom cm}^{-2}$), being the same for all samples. The samples used for Raman measurements consist of a Si buffer layer with a thickness of 100 nm, followed by 5 periods of 6 ML Ge layers separated by 50 nm Si spacers and a 20 nm Si cap layer. The growth temperatures were 500 and 700°C for the cap and buffer Si layers, respectively. Immediately after the deposition of Ge, the temperature was lowered to $T_s = 350\text{--}400^\circ\text{C}$ and the Ge islands are covered by a 2 nm Si layer at that temperature. This is necessary to preserve the shape and size of the Ge islands with subsequent Si capping at higher T_s [14]. The growth of the Ge layers was monitored by reflection high-energy electron diffraction where the transition from two-dimensional to three-dimensional island growth was observed after ~ 4 ML of Ge deposition.

3. Experimental results

3.1. Scanning tunnelling microscopy

Scanning tunnelling microscopy (STM) of samples without the Si cap layer was used to assess the morphology of Ge layers. Figure 1 shows a series of images taken at different Ge deposition rates, and the lateral size histograms derived for each image. Although, some of the islands did not have a square base, we used their geometrical mean, $l = \sqrt{a \times b}$ (a and b are the island base lengths), as a convenient measure of their size. The island size distribution was evaluated by measuring the lateral dimensions on $200 \times 200 \text{ nm}^2$ or $200 \times 400 \text{ nm}^2$ scans dependent on the sample until more than 100 islands were taken into consideration. From these data, the width of the size distribution, σ , was calculated as standard deviation,

$$\sigma^2 = \frac{1}{n-1} \sum_{i=1}^n (l_i - \langle l \rangle)^2,$$

where n is the number of islands evaluated, and $\langle l \rangle$ is the mean size. The parameters of Ge QDs distribution obtained

from the analysis of STM images are listed in table 1. The average island size decreases with increasing growth rate while the normalized width of size distribution $\sigma/\langle l \rangle$ shows nonmonotonic behaviour. Simultaneously, the island density increases with R due to increasing surface concentration of migrating Ge atoms and, thus, the number of island nuclei [15]. These results are in good qualitative agreement with those obtained previously by Cho *et al* [12], Schwarz–Selinger *et al* [16] and Abstreiter *et al* [17].

From the STM images, we observe that the Ge nanoclusters grown at a low deposition rate have the shape of ‘hut’ clusters bounded by $\{105\}$ facets [18] with rectangular or square bases in two orthogonal orientations, corresponding to $\langle 100 \rangle$ directions in the substrates. At the highest R , the formation of elongated islands is suppressed and square-based pyramids dominate, giving rise to a more narrow size distribution. In this case the faster Ge deposition promotes nucleation of additional square-based islands, in preference to the diffusion of absorbed Ge atoms to existing islands causing subsequent elongation.

3.2. Raman spectroscopy

The samples were also characterized by Raman spectroscopy to estimate the Ge–Si intermixing effect in Ge QDs and the elastic strain in them. The Raman spectra were measured at room temperature using a computer-controlled setup based on a DFS-52 spectrometer (LOMO, St. Petersburg); an Ar^+ laser ($\lambda = 514.5 \text{ nm}$) was used as the pump for the Raman process. We used quasi-backscattering geometry, the incident radiation was polarized along the $\langle 100 \rangle$ crystallographic direction, and the scattered light was detected in $\langle 010 \rangle$ polarization. The chosen configuration is allowed for the scattering by longitudinal optical phonons in Ge and Si and forbidden for the two-phonon scattering by transverse acoustical phonons in the Si substrate.

Raman spectra of samples with Ge layers grown at different R are shown in figure 2. A peak observed at

Table 1. The surface density of Ge nanoclusters n_{QD} , the Ge island mean size in the growth plane $\langle l \rangle$, and the normalized standard deviation of size distribution $\sigma/\langle l \rangle$ in layers of Ge islands fabricated at different deposition rates R and evaluated from STM images. The amount of Ge deposited θ and the channelling minimum yield χ_{min} of Ge ($\chi_{\text{min}}^{\text{Ge}}$) were obtained in Rutherford backscattering/channelling experiments. c is the Ge content and ϵ_{xx} is the average lateral strain in Ge islands determined from Raman measurements.

R (ML s $^{-1}$)	n_{QD} (cm $^{-2}$)	$\langle l \rangle$ (nm)	$\sigma/\langle l \rangle$	θ (ML)	$\chi_{\text{min}}^{\text{Ge}}$ (%)	c	ϵ_{xx}
0.02	$(1.5 \pm 0.2) \times 10^{11}$	14.1	0.21	5.4 ± 0.5	6.5	0.75	-0.029
0.2	$(3.2 \pm 0.3) \times 10^{11}$	10.1	0.27	6.1 ± 0.5	4.0	0.83	-0.030
2	$(3.6 \pm 0.3) \times 10^{11}$	9.8	0.19	7.1 ± 0.5	<3	0.88	-0.035

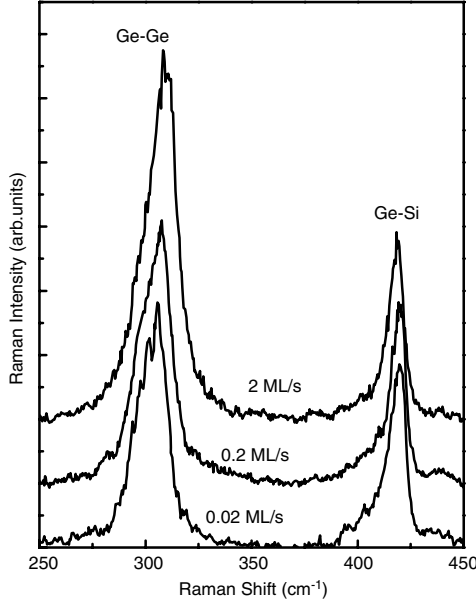


Figure 2. Raman spectra of the samples with the layers of Ge QDs grown at various Ge deposition rates R .

~ 300 cm $^{-1}$ originates from the optical vibration of Ge-Ge bonds in Ge islands. Another feature at ~ 420 cm $^{-1}$ corresponds to the local Ge-Si vibrations. Based on Raman measurements the Ge-Si intermixing effect is usually found from the ratio of the integrated intensities of the Ge-Ge and Ge-Si peaks using the following expression [19, 20]

$$\frac{I_{\text{Ge-Ge}}}{I_{\text{Si-Ge}}} = \alpha \frac{c}{2(1-c)}, \quad (1)$$

where c is the Ge content in GeSi nanoclusters or films and α is a constant which depends on the experimental conditions. We initially checked the validity of (1) for a number of continuous $\text{Si}_{1-c}\text{Ge}_c$ layers with a Ge composition known from x -ray diffraction measurements. In this way, we determined a coefficient α of 2 for our experimental setup. Note that equation (1) disregards the possible influence of the boundary between the GeSi alloy and Si environment on the intensity of the Ge-Si signal and hence gives the proper results only for thick films.

Here, we establish the relation between the integrated intensities of the Ge-Ge and Ge-Si Raman peaks and the Ge content in thin $\text{Ge}_c\text{Si}_{1-c}$ nanoclusters, in which the influence of heterointerface GeSi/Si on the Raman spectra should be taken into account. Since the aspect ratio of GeSi islands under study is much less than unity ($h/l \approx 0.1$ for ‘hut’ clusters

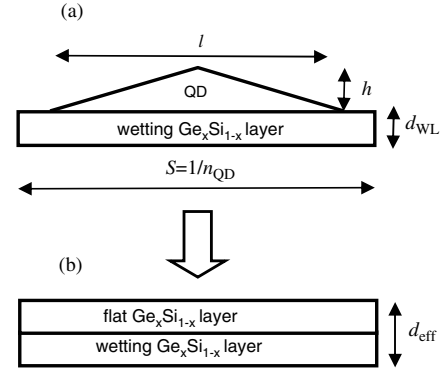


Figure 3. A model which describes the flat-layer approximation used for the estimation of QD composition.

bounded by $\{105\}$ facets, here l is the island lateral size and h is its height) we may use the flat-layer approximation. Let us consider an array of GeSi pyramids lying on a wetting layer with a thickness d_{WL} and surrounded with Si. Let us divide the array into separate regions with area $S = 1/n_{\text{QD}}$, where n_{QD} is the QD density. Each such region contains one $\text{Ge}_c\text{Si}_{1-c}$ pyramid (figure 3(a)). Now we replace the system ‘pyramid plus wetting layer’ by a flat $\text{Ge}_c\text{Si}_{1-c}$ film with an effective thickness $d_{\text{eff}} = d_{\text{WL}} + (l^2h/3)n_{\text{QD}}$ to conserve the total volume of the system (figure 3(b)). Note that d_{eff} measured in monolayers is θ/c , where θ is the amount of Ge deposited. For a random alloy, the fraction of nearest neighbour Ge-Si pairs in alloy is $2c(1-c)$, the fraction of nearest neighbour Ge atoms is c^2 , and the fraction of nearest neighbour Ge-Si pairs on the boundary between the $\text{Ge}_c\text{Si}_{1-c}$ film and Si matrix is c (notice there are two such boundaries, top and bottom). Then the total number of Ge-Ge and Ge-Si pairs is

$$N_{\text{Ge-Ge}} = c^2(\theta/c-1), \quad N_{\text{Ge-Si}} = 2c+2c(1-c)(\theta/c-1), \quad (2)$$

respectively. Since the ratio of the integrated intensities of the Ge-Ge and Ge-Si peaks $I_{\text{Ge-Ge}}/I_{\text{Ge-Si}}$ is proportional to the ratio $N_{\text{Ge-Ge}}/N_{\text{Ge-Si}}$, we arrive at

$$\frac{I_{\text{Ge-Ge}}}{I_{\text{Ge-Si}}} = \alpha \frac{N_{\text{Ge-Ge}}}{N_{\text{Ge-Si}}} = \alpha \frac{(\theta-c)}{2[1+(c^{-1}-1)(\theta-c)]}. \quad (3)$$

For $\theta \rightarrow \infty$, equation (3) reduces to (1), which is a well-known expression for thick GeSi layers.

The values of c obtained from the Raman spectra and equation (3) are listed in table 1. Analysis shows that the average Ge content in the dots increases with increasing deposition rate. Similar behaviour has previously been reported for dome-shaped Ge islands fabricated at 620–650 °C [13, 21]. Since the amount of Ge deposited as well

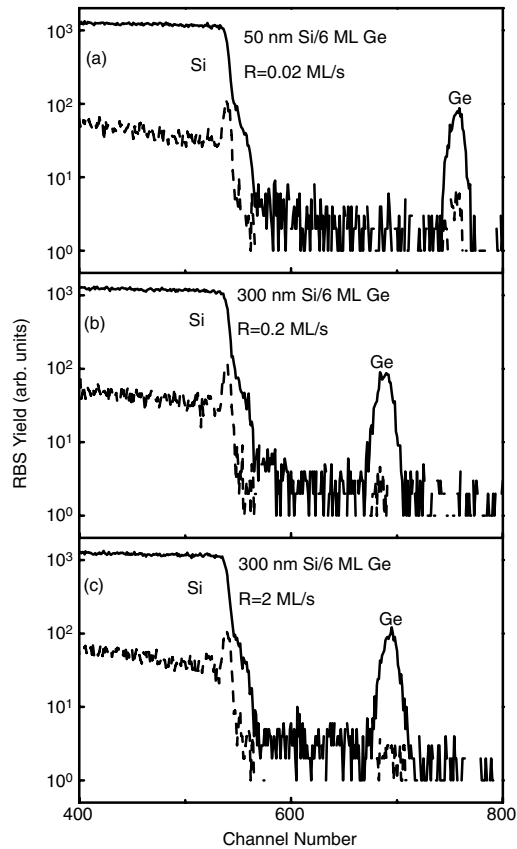


Figure 4. Random (solid lines) and aligned (broken lines) backscattering spectra of Si/Ge/Si(001) heterostructures with Ge nanoclusters deposited at (a) $R = 0.02 \text{ ML s}^{-1}$, (b) $R = 0.2 \text{ ML s}^{-1}$, and (c) $R = 2 \text{ ML s}^{-1}$.

as the growth and overgrowth temperatures are the same for all three samples this finding provides evidence that intermixing in self-organized GeSi QDs proceeds by a surface diffusion process [21–23] rather than a bulk interdiffusion mediated by nonuniform stress fields [24–26].

The average lateral strain ϵ_{xx} ($=\epsilon_{yy}$) in Ge nanoclusters can be estimated from the Ge–Ge phonon frequency $\omega_{\text{Ge-Ge}}$ using the following empirical relation [27]

$$\omega_{\text{Ge-Ge}} = 300.3 - 32(1-c) + 12(1-c)^2 - (450 - 30c)\epsilon_{xx}. \quad (4)$$

Here we neglect the size-confinement effect of optical phonons which has to be important for QDs of smaller sizes [28]. This leads to some underestimation of ϵ_{xx} . The data are presented in table 1. The negative strain values indicate a compressive lateral strain within Ge islands. In the sample with the largest R the Ge dots are the most strained with ϵ_{xx} being close to the maximum biaxial compressive strain for pure Ge islands in Si(001) (≈ 0.04), whereas when the Ge was deposited at a smaller rate the strain is relaxed due to the Ge–Si intermixing. Moreover, one could expect that the strain would increase with increasing deposition rate on the basis of island–island elastic interactions, i.e., at higher deposition rates, the island density increases so that the islands interact more strongly and relax less effectively via the inhomogeneous strains allowed for isolated islands.

3.3. Rutherford backscattering measurements

Rutherford backscattering spectroscopy (RBS) was used to estimate the amount of Ge deposited and to characterize qualitatively the degree of strain relaxation in the Ge layer. RBS experiments were performed at the Research Center Rossendorf using $^4\text{He}^+$ beams with a beam energy of 1.2 MeV. Usually, the channelling minimum yield, χ_{min} , which is a ratio of the backscattering yield when the impinging beam is aligned to a crystallographic axis to that for a random beam incidence, is considered as a measure of the crystalline quality of the films. For a perfect crystal of Si(001), χ_{min} is about 3%. Figure 4 shows the RBS/channelling spectra of samples fabricated at different Ge growth rates R . The thickness of the Si capping layer is 300 nm when $R = 0.2 \text{ ML s}^{-1}$ and 2 ML s^{-1} , and 50 nm for the sample with $R = 0.02 \text{ ML s}^{-1}$. In all samples, the Ge coverage is determined to be about 6 ML (see table 1) in good agreement with the measurements of Ge flux *in situ* by a quartz thickness monitor. The minimum yield from the Si matrix taken immediately under the surface peak is about 2.6% independent of the growth conditions and corresponds to a high quality Si structure. An important feature is the reduction of χ_{min} of the buried Ge layer with increasing Ge deposition rate. At $R = 2 \text{ ML s}^{-1}$, $\chi_{\text{min}}^{\text{Ge}}$ approaches that of the best Si crystals, implying that in this case Ge atoms occupy positions of Si atoms and, hence, the Ge layer is nearly fully strained, as also observed in Raman measurements.

4. Conclusions

Results from a study of the effect of Ge deposition rate on the morphology and composition of hut-shaped Ge clusters grown on (001) Si at 500°C are reported in detail. We found that properties of Ge islands such as the average lateral size, the width of the size distribution, and the island composition are improved by increasing the deposition rate. The highest value of Ge flux used in this work was 2 ML s^{-1} . It takes only 3 s to grow a 6 ML thick Ge layer. For this reason, we think that rates greater than 2 ML s^{-1} are not practical for further tuning the structural properties of self-assembled Ge/Si nanoislands produced by molecular-beam epitaxy.

Acknowledgments

The authors are much obliged to S A Teys for STM experiments. We acknowledge the support of RFBR (Grant No. 06-02-16143), State Contract No. 02.442.11.7282, and INTAS (Grant No. 03-51-5051).

References

- [1] Drucker J and Chaparro S 1997 *Appl. Phys. Lett.* **71** 614
- [2] Denker U, Stoffel M, Schmidt O G and Sigg H 2003 *Appl. Phys. Lett.* **82** 454
- [3] Chaparro S A, Zhang Y, Drucker J, Chandrasekhar D and Smith D J 2000 *J. Appl. Phys.* **87** 2245
- [4] Tersoff J, Teichert C and Lagally M G 1996 *Phys. Rev. Lett.* **76** 1675
- [5] Mateeva E, Sutter P, Bean J C and Lagally M G 1997 *Appl. Phys. Lett.* **71** 3233
- [6] Thanh V L, Yam V, Boucaud P, Zheng Y and Bouchier D 2000 *Thin Solid Films* **369** 43

- [7] Peng C S, Huang Q, Cheng W Q, Zhou J M, Zhang Y H, Sheng T T and Tung C H 1998 *Phys. Rev. B* **57** 8805
- [8] Portavoce A, Volpi F, Ronda A, Gas P and Berbezier I 2000 *Thin Solid Films* **380** 164
- [9] Zhu J, Brunner K and Abstreiter G 1998 *Appl. Phys. Lett.* **73** 620
- [10] Nikiforov A I, Ulyanov V V, Pchelyakov O P, Tiis S A and Gutakovskii A K 2005 *Phys. Solid State* **47** 67
- [11] Dvurechenskii A V, Smagina J V, Zinovyev V A, Teys S A, Gutakovskii A K and Groetzschel R 2004 *Int. J. Nanosci.* **3** 19
- [12] Cho B, Schwarz-Selinger T, Ohmori K, Cahill D and Greene J E 2002 *Phys. Rev. B* **66** 195407
- [13] McDaniel E P, Jiang Q, Crozier P A, Drucker J and Smith D J 2005 *Appl. Phys. Lett.* **87** 223101
- [14] Wu Y Q, Li F H, Cui J, Lin J H, Wu R, Qin J, Zhu C Y, Fan Y L, Yang X J and Jiang Z M 2005 *Appl. Phys. Lett.* **87** 223116
- [15] Kamins T I, Carr E C, Williams R S and Rosner S J 1997 *J. Appl. Phys.* **81** 211
- [16] Schwarz-Selinger T, Foo Y L, Cahill D G and Greene J E 2002 *Phys. Rev. B* **65** 125317
- [17] Abstreiter G, Schittenhelm P, Engel C, Silveira E, Zrenner A, Meertens D and Jäger W 1996 *Semicond. Sci. Technol.* **11** 1521
- [18] Mo Y-M, Savage D E, Swartzentruber B S and Lagally M G 1990 *Phys. Rev. Lett.* **65** 1020
- [19] Mooney P M, Dacol F H, Tsang J C and Chu J O 1993 *Appl. Phys. Lett.* **62** 2069
- [20] Tsang J C, Mooney P M, Dacol F and Chu J O 1994 *J. Appl. Phys.* **75** 8098
- [21] Yakimov A I, Dvurechenskii A V, Volodin V A, Efremov M D, Nikiforov A I, Mikhalyov G Yu, Gatskevich E I and Ivlev G D 2005 *Phys. Rev. B* **72** 115318
- [22] Katsaros G, Costantini G, Stoffel M, Esteban R, Bittner A M, Rastelli A, Denker U, Schmidt O G and Kern K 2005 *Phys. Rev. B* **72** 195320
- [23] Denker U, Stoffel M and Schmidt O G 2003 *Phys. Rev. Lett.* **90** 196102
- [24] Ratto F, Rosei F, Locatelli A, Cherifi S, Fontana S, Heyn S, Szkutnik P-D, Sgarlata A, De Crescenzi M and Motta N 2005 *J. Appl. Phys.* **97** 043516
- [25] Chaparro S A, Drucker J, Zhang Y, Chandrasekhar D, McCartney M R and Smith D J 1999 *Phys. Rev. Lett.* **83** 1199
- [26] Liao X Z, Zou J, Cockayne D J, Qin J, Jiang Z M, Wang X and Leon R 1999 *Phys. Rev. B* **60** 15605
- [27] Floyd M, Zhang Y, Driver K P, Drucker J, Crozier P A and Smith D J 2003 *Appl. Phys. Lett.* **82** 1473
- [28] Volodin V A, Efremov M D, Deryabin A S and Sokolov L V 2006 *Semiconductors* **40** accepted
- [29] Kwok S H, Yu P Y, Tung C H, Zhang Y H, Li C S, Peng C S and Zhou J M 1999 *Phys. Rev. B* **59** 4980